ACS APPLIED NANO MATERIALS

www.acsanm.org Article

fM−aM Detection of the SARS-CoV-2 Antigen by Advanced Lateral Flow Immunoassay Based on Gold Nanospheres

Yilin Liu, Li Zhan, Jesse W. Shen, Bàrbara Baro, Andrea Alemany, James Sackrison, Oriol Mitjà, and John C. Bischof*

Cite This: *ACS Appl. Nano Mater.* 2021, 4, 13826−13837 Read Online

ACCESS | Metrics & More | Article Recommendations | Supporting Information

ABSTRACT: The SARS-CoV-2 global pandemic created an unprecedented need for rapid, sensitive, and inexpensive point-of-care (POC) diagnostic tests to treat and control the disease. Many POC SARS-CoV-2 lateral flow immunoassays (LFAs) have been developed and/or commercialized, but with only limited sensitivity (μM−fM). We created an advanced LFA based on gold nanospheres (GNSs) with comprehensive assay redesign for enhanced specific binding and thermal contrast amplification (TCA) on GNSs for signal amplification, which enabled fM−aM detection sensitivity for SARS-CoV-2 spike receptor-binding domain (RBD) proteins within 30 min. The advanced LFA can visually detect RBD proteins down to 3.6 and 28.6 aM in buffer and human nasopharyngeal wash, respectively. This is the first reported LFA achieving sensitivity comparable to that of the PCR (aM−zM) by visual reading, which was much more sensitive than traditional LFAs. We also developed a fast (<1 min) TCA reading algorithm, with results showing that this TCA could distinguish 26−32% visual false negatives for clinical commercial LFAs. When our advanced LFAs were applied with this TCA, the sensitivities were further improved by eightfold to 0.45 aM (in buffer) and 3.6 aM (in the human nasopharyngeal wash) with a semiquantitative readout. Our proposed advanced LFA with a TCA diagnostic platform can help control the current SARS-CoV-2 pandemic. Furthermore, the simplicity and speed with which this assay was assembled may also facilitate preparedness for future pandemics.

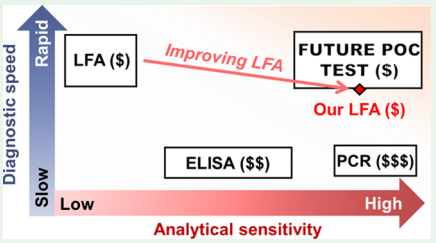

KEYWORDS: *SARS-CoV-2, lateral flow immunoassay, sensitivity, thermal contrast amplification, assay optimization*

INTRODUCTION

The past decades have witnessed a recurrence of multiple pandemics such as severe acute respiratory syndrome (SARS), Middle East respiratory syndrome coronavirus (MERS), H1N1 and other influenza viruses, the Ebola virus, the Zika virus, and, most recently, the SARS-CoV-2 virus.[1,2] A recurring issue in the response to these pandemics is the lack of rapid, accurate, and affordable diagnostic tests to efficiently prevent and control the spread of the disease.[3] The SARS-CoV-2 pandemic has caused significant global morbidity and mortality. As of 13 July 2021, there have been over 186 million confirmed cases and over 4 million cumulative deaths worldwide due to SARS-CoV-2.[4] To control the spread, multiple testing methods have been developed and applied, such as the RT-PCR, rapid tests (*i.e.*, lateral flow immunoassays, LFAs), the CRISPR-based assay, and diagnostic imaging (*e.g.*, computed tomography on patients' lungs).[5−7] The reverse transcription-polymerase chain reaction (RT-PCR) is one of the most widely used methods due to its ultrahigh sensitivity, but it usually has a long turnaround time and requires expensive reagents, equipment, and professional training.[3,8] While its claimed assay time can be less than an hour, the actual time to diagnose a patient suspected with SARS-CoV-2 infection was >24 h or even several days during outbreaks due to the need to ship samples to laboratories and the limited available testing resources (*i.e.*, facilities, reagents, and professionals).[3] In addition, many underdeveloped countries lack sufficient resources and budget to carry out population-wide RT-PCR tests.[9,10]

Serological and antigen rapid tests were developed and commercialized to address these difficulties and help relieve the diagnostic burden. While these rapid LFA tests are faster, cheaper, and easier to use than the RT-PCR, their performance results have been inconsistent, with a notable lack of sensitivity and no quantification. Some cohort studies showed good sensitivity of commercial serological and antigen rapid tests when comparing results with confirmatory RT-PCR results,[11−14] but unsatisfactory diagnostic performance was also reported. The Coris SARS-CoV-2 Ag Respi-Strip test, for example, showed sensitivity as low as 30.2% for clinical samples,[15] and the BinaxNOW antigen rapid test cards were reported to have an analytical sensitivity approximately equivalent to the cycle threshold of 29−30 from a generic qRT-PCR, which may not be sufficient to detect all relevant

Received: October 3, 2021
Accepted: December 2, 2021
Published: December 14, 2021

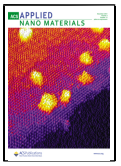

https://doi.org/10.1021/acsanm.1c03217
ACS Appl. Nano Mater. 2021, 4, 13826−13837

Table 1. Detection Sensitivity and Assay Time of the Reported SARS-CoV-2 Antigen and Antibody Rapid Tests[a,b]

			limit of detection (LoD)			
analytes	LFA improvement	sample matrix	mass concentration	molarity	assay time (min)	refs
IgG	fluorescence	diluted serum by buffer	NA		10	30
IgG/IgM	fluorescence	buffer	NA. 10^4-fold better than visual reading with colloidal gold		15	31
IgG/IgM	fluorescence	serum	IgM: 0.236 μg/mL; IgG: 0.125 μg/mL	IgM: 0.26 nM IgG: 0.83 nM	10	32
IgG/IgM	SERS	diluted serum by buffer	1 pg/mL (IgG or IgM)		NA	33
IgG	scattering contrast	buffer	0.1 ng/mL		NA	34
γ-radiated SARS-CoV-2	antibody paired with ACE2	buffer	1.86×10^5 copies/mL	0.3 fM	20	35
S- & N-proteins	NA	NA (nonclinical)	S: 1 ng/mL; N: 0.1 ng/mL	S: 5.71 pM[b] N: 0.88 pM[b]	11	36
N-protein	NA	diluted serum by buffer	0.65 ng/mL	5.7 pM[b]	20	37
spike RBD protein	TCA	a. buffer b. nasopharyngeal wash (human)	a: 0.016 fg/mL b: 0.125 fg/mL	a: 0.45 aM b: 3.6 aM	30	this study
	NA		a: 0.125 fg/mL b: 1 fg/mL	a: 3.6 aM b: 28.6 aM		

[a]NA: not applicable; SERS: surface-enhanced Raman scattering; ACE2: angiotensin-converting enzyme 2; S-protein: spike protein; N-protein: nucleocapsid protein; RBD: receptor-binding domain; and TCA: thermal contrast amplification. [b]Assume that the molecular weights for SARS-CoV-2 spike and nucleocapsid proteins are 175 and 114 kDa, respectively, when they were not notified in the literature.

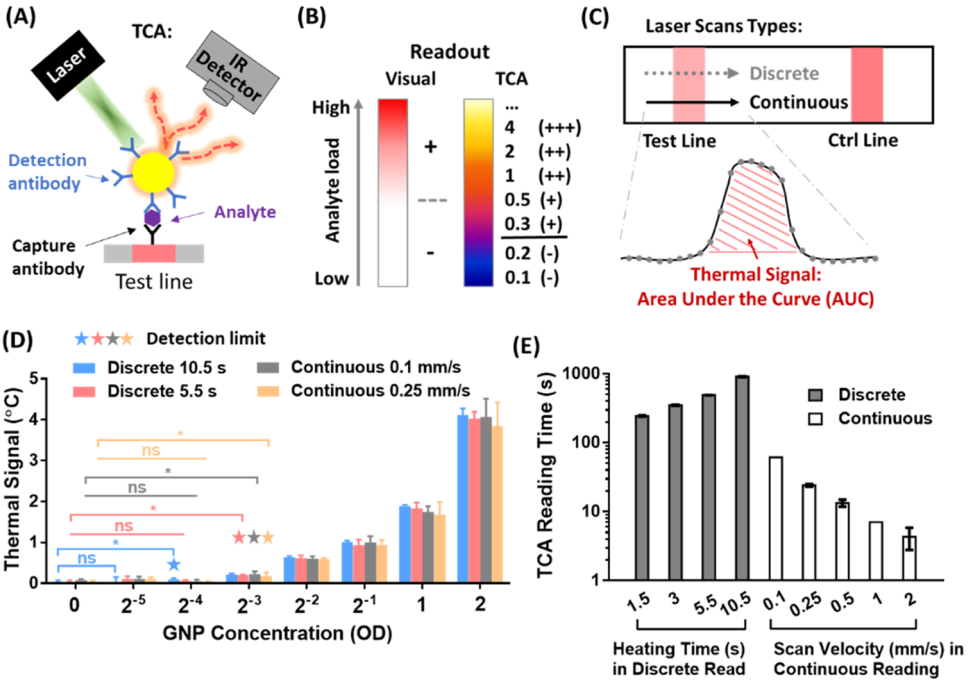

Figure 1. Building and characterizing a fast TCA reader by continuous reading. (A) Schematic working mechanism of TCA, where gold nanoparticles are excited under laser irradiation and their elevated temperature is recorded by an infrared (IR) camera. (B) Readout formats by visual with qualitative results (±) *vs* TCA with semiquantitative (numeric) results, where strong, medium, or weak signal can correlate to the antigen load. (C) Schematic of discrete (slow) and continuous (fast) reading algorithms in a TCA reader. The thermal signal of a test line was obtained by calculating the area under the temperature curve, recorded by an IR camera when scanning across the test line. (D) Thermal signals of test lines from calibration LFAs, read by both continuous and discrete reading algorithms in the TCA reader. In discrete reading, the heating time per point included 5.5 and 10.5 s. For continuous scans, the scan velocity included 0.1 and 0.25 mm/s. The test lines were printed with various concentrations of gold nanospheres (GNSs), which were characterized by the peak absorbance (unit: OD, optical density) for a 1 cm path length of light through their solutions. (E) Measured time consumption per reading by both discrete and continuous reading algorithms. For discrete readings, the heating time per point ranged from 1.5 to 10 s. In continuous reading, the scan velocity ranged from 0.1 to 2 mm/s. For all reading conditions, the number of replicates was three. The statistical significance is indicated with asterisks: ns: $p > 0.05$; *$p < 0.05$.

infections.[16] A similar issue of low sensitivities of rapid antigen and antibody tests was reported elsewhere, and these tests were less recommended for diagnosing acute SARS-CoV-2 infection.[17−20] In short, the commercial rapid antigen and antibody tests remain of limited usefulness for detecting all relevant SARS-CoV-2 infections, and thus cannot fully serve the immediate response to and management of the pandemic spreading worldwide.[3]

To better detect SARS-CoV-2 infections at the point-of-care (POC), many research efforts have been put to improving the sensitivity of commercial LFAs.[21−23] Table 1 shows the recent literature applying either signal amplification methods (*e.g.*, fluorescence and surface-enhanced Raman scattering) or assay

https://doi.org/10.1021/acsanm.1c03217
ACS Appl. Nano Mater. 2021, 4, 13826−13837

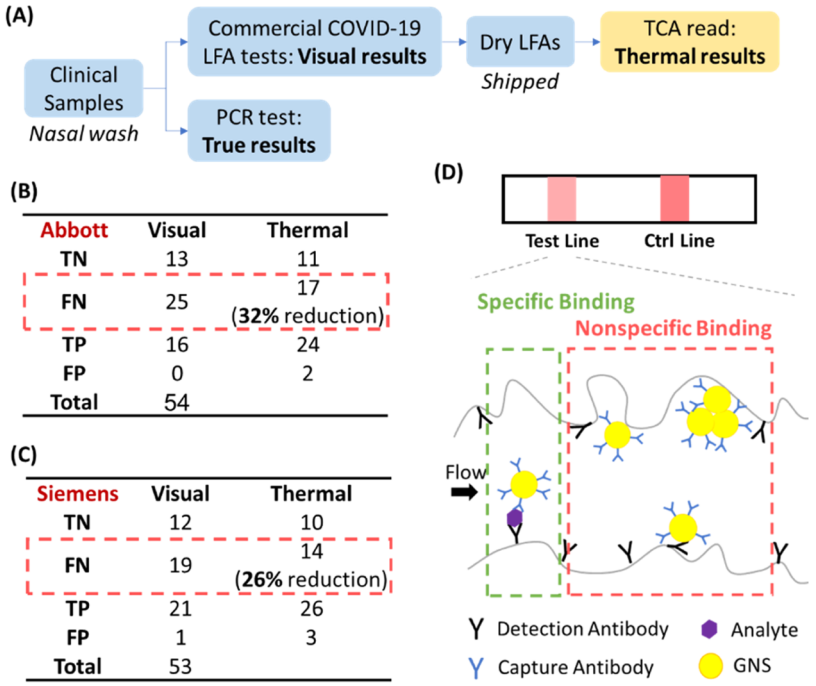

Figure 2. TCA reading of commercial SARS-CoV-2 antigen LFAs and illustration of specific and nonspecific binding in LFAs. (A) Schematic flowchart for testing clinical SARS-CoV-2 samples by PCR, commercial visual SARS-CoV-2 antigen LFAs, and thermal contrast amplification (TCA) LFA reading. (B, C) Statistics of visual and thermal results of (B) Abbott and (C) Siemens SARS-CoV-2 antigen LFAs tested with clinical samples. PCR results were taken as true negative and true positive results for comparison. (D) Schematic of specific binding occurring with nonspecific binding at test lines. Legends for B and C include TN: true negative; FN: false negative; TP: true positive; and FP: false positive.

improvement (*e.g.*, novel affinity molecules) to LFAs for better detection of SARS-CoV-2. Most had assay time between 10 and 20 min and detection sensitivity in the nM−fM (*i.e.*, 10^{-9}−10^{-15} M) range, still much lower than RT-PCR (aM−zM, or 10^{-18}−10^{-21} M). Although it is recently reported that LFA read by scanning electron microscopy (SEM) could achieve sensitivity comparable to RT-PCR,[24] the testing platform is too complicated and expensive for POC use.

Meanwhile, assays with sample enrichment and LFA readout have been under rapid development, aiming for more accurate POC tests. The reverse transcript loop-mediated isothermal amplification LFA (RT-LAMP-LFA) system, for example, can detect SARS-CoV-2 RNA at concentrations of ≥2 copies/μL (3 aM) in 40 min.[25] Similar work used various isothermal amplification methods coupled with an LFA readout, whose detection sensitivity was aM−zM with assay time from approximately 30 min−1 h.[26−29] These are promising for future POC use to replace traditional PCR tests, especially for population screening in epidemics. However, challenges for these isothermal amplification LFA platforms still exist and need to be addressed for future POC use.[21] Compared with LFAs, for example, these assays need more expensive reagents, multiple steps, and isothermal incubators, and have less tolerance to contamination.[21]

To overcome these challenges, we established an advanced LFA based on gold nanospheres (GNSs) with thermal contrast amplification (TCA) to detect the spike SARS-CoV-2 receptor-binding domain (RBD) antigen for acute infection. To break through the fM detection limit of current LFAs, we carried out comprehensive assay optimization along with signal amplification (*i.e.*, TCA). Specifically, we use high-affinity antibodies, optimal running buffer, large GNSs, and an improved conjugation method with increased antigen-binding sites for enhanced specific binding (SB), along with TCA reading where the GNSs captured at test lines were laser-excited to generate the amplified photothermal signals. As a result, the advanced LFAs in this work provided 3.6 and 28.6 aM detection limits readable with the naked eye to test the RBD proteins in buffer and human nasopharyngeal wash, respectively. This is the first report on an advanced LFA achieving fM−aM analytical sensitivity that can be read with the naked eye, which was much more sensitive than conventional LFAs and even comparable to PCR's sensitivity range.[21] Table 1 shows its advantage in detection sensitivity to SARS-CoV-2 over other LFAs from the literature. Meanwhile, a fast (<1 min) TCA reading was developed and identified 26−32% visual false negatives from clinical commercial LFAs. When we applied this TCA to our advanced LFAs, the detection limits were further lowered to 0.45 aM (in buffer) and 3.6 aM (in human nasopharyngeal wash) in a semi-quantitative readout format. The advanced LFAs with TCA can help prevent the recurrence of the current SARS-CoV-2 pandemic and may also better prepare the world to diagnose and control the spread of other diseases and prevent future pandemics.

RESULTS AND DISCUSSION

TCA: Faster Reading Without Loss of Accuracy. TCA can improve the sensitivities of LFAs although the throughput of the traditional reading algorithm needs improvement. With TCA, the captured gold nanoparticles at a test line were excited by laser irradiation and showed stronger photothermal effects than the background membrane, enabling the detection of subvisual positives (Figure 1A).[38−43] As a result, TCA reading improved the sensitivities of clinical commercial LFAs to diagnose group A *Streptococcus* and influenza A and B in

https://doi.org/10.1021/acsanm.1c03217
ACS Appl. Nano Mater. 2021, 4, 13826−13837

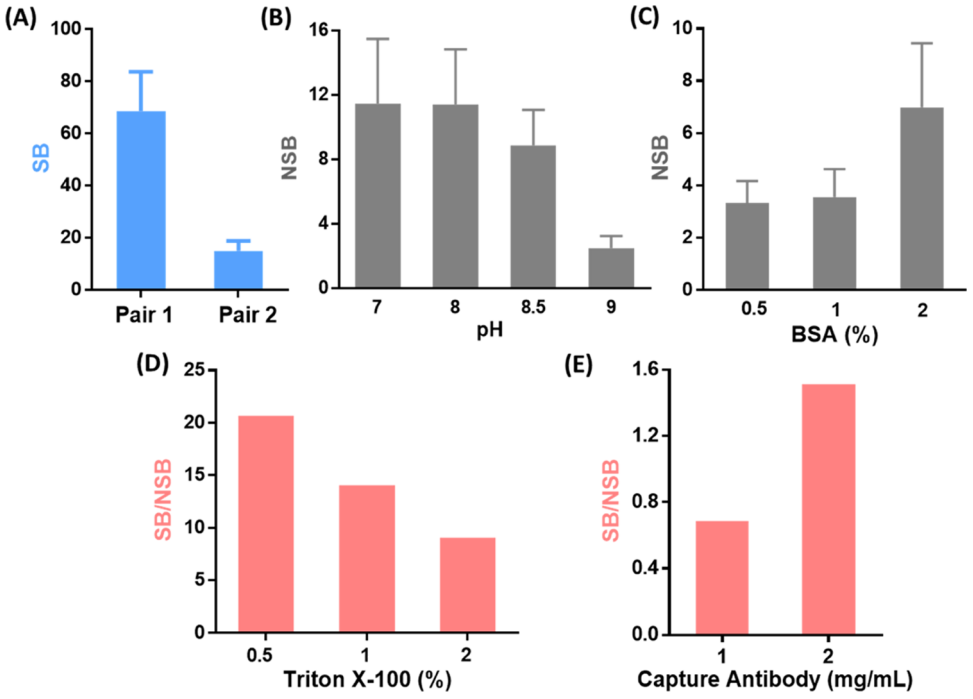

Figure 3. Optimizing antibody and buffer for SARS-CoV-2 spike receptor-binding domain (RBD) protein LFA. (A) Comparison of SB of two antibody pairs (Hytest and MyBioSource; see Materials for details) to the RBD protein in an LFA format. The first pair was used in the following assay optimization work. (B) Effects of buffer pH on NSB. The concentrations of BSA, Triton X-100, NaCl, and ProClin 300 in buffer were 0.5%, 0.5%, 0.15 M, and 0.05%, respectively. (C) Effects of the BSA concentration in running buffer on NSB. The pH and the concentrations of Triton X-100, NaCl, and ProClin 300 in buffer were 9, 1%, 0.15 M, and 0.05%, respectively. (D) Effects of the Triton X-100 concentration in running buffer on the SB/NSB ratio. The pH and the concentrations of Triton X-100, NaCl, and ProClin 300 in buffer were 9, 1%, 0.15 M, and 0.05%, respectively. (E) Optimizing concentration of the capture antibody at test lines by comparing SB/NSB ratios. The SB and NSB in panel (E) were thermal signals from thermal contrast amplification (TCA) reading of test lines, while those in (A–D) were grayscale intensities, calculated as the area above the grayscale curves across test lines plotted in ImageJ. NSB or SB was noise or signal of a test line when an LFA was run with blank or antigen-loaded buffers, respectively. The antigen concentrations were controlled as the same for each set of studies in panels (A), (D), and (E), respectively.

previous cohort studies.[43,44] TCA reading also showed a semiquantitative readout in diagnosing C-reactive proteins and HIV p24 proteins,[41,42] whose numerical thermal signals increased with increasing antigen load (Figure 1B). However, the old discrete algorithm for TCA reading (*i.e.*, point-by-point reading across a test line, as shown in Figure 1C), used in the previous studies,[38−43] took about 15−20 min for one reading of an LFA.

To boost throughput, we developed a fast and continuous reading algorithm (Figure 1C), allowing times of <1 min per reading with comparable performance to the traditional discrete reading type. Characterization of the fast-reading algorithm was conducted by reading calibration LFAs (detailed in Section S1 in the Supporting Information). Thermal signals and time consumption are shown in Figure 1D,E. In Figure 1D, both reading algorithms showed semiquantitative thermal signals corresponding to concentrations of GNSs at test lines. Figure 1D also shows that the continuous reading, with either a 0.1 or 0.25 mm/s scan velocity, had a similar limit of detection (LoD) for GNSs (2^{-3} optical density, OD) to the discrete reading with 5.5 s heating time per point. Although the discrete heating with 10.5 s heating time had a twofold lower LoD (2^{-4} OD), its reading time was >15 min, significantly longer than that of the continuous reading (as low as <1 min), as shown in Figure 1E. While increasing scan velocity can further reduce reading time, scans that are too quick may miss some information from real LFAs, which are expected to be more complex than calibration LFAs. Therefore, in this study, a 0.25 mm/s scan velocity was used to continuously read both commercial and lab prototype LFAs, with reading time <1 min.

Clinical Commercial SARS-CoV-2 LFAs: Reduction of False Negatives by TCA. To benchmark the improved performance of our new SARS-CoV-2 antigen LFA, we performed a baseline test of selected existing clinical commercial SARS-CoV-2 LFAs by visual and TCA reading. Results showed a reduction in false negatives to diagnose clinical samples by TCA over visual reading on PanBio SARS-CoV-2 Ag Rapid LFAs from Abbott and CLINITEST Rapid SARS-CoV-2 Antigen LFAs from Siemens. Comparison of visual and thermal results in Figure 2B,C showed that TCA detected about 32 and 26% visual false negatives from Abbott and Siemens SARS-CoV-2 antigen LFAs, respectively. Thermal signals of the visually false negatives identified by TCA are plotted in Figure S1. This improved sensitivity of commercial SARS-CoV-2 antigen LFAs by TCA is also consistent with our previous cohort studies for rapid diagnosis of influenza[43] and group A: *Streptococcus*.[44]

TCA also slightly increased false positives for both Abbott and Siemens LFAs, as shown in Figures 2B,C and S1. This is mainly due to amplified noise from nonspecific binding (NSB) at test lines by TCA.[43] It is known that NSB usually exists along with SB in LFAs, corresponding to noise and signal, respectively. As shown in Figure 2D, NSB can arise from different side reactions, including the hydrophobic and

https://doi.org/10.1021/acsanm.1c03217
ACS Appl. Nano Mater. 2021, 4, 13826−13837

electrostatic interactions of GNS conjugates with capture antibodies and/or with the membrane, and the physical capture of GNS aggregates in the membrane.[42,45,46] The accumulation of NSB can therefore cause false positives in visual reading. This issue can be even more apparent after signal amplification, thus setting a limit to sensitivity improvement for various signal amplification methods.[21] To reduce NSB and false positives, extensive assay optimization is needed to fit with signal amplification. With a redesign of the assay, for example, the LFA with TCA achieved ELISA-level sensitivity (~pM) in detecting HIV p24 proteins.[42]

In short, while it creates some false positives, TCA can reduce visual false negatives in commercial LFAs. To dramatically improve sensitivity (≤fM) and suppress possible false positives from cross-reactions between built-up reagents, we developed advanced ultrasensitive SARS-CoV-2 antigen LFAs by comprehensive assay optimization for maximal SB and minimal NSB with signal amplification (TCA).

LFA Redesign I: Antibody and Buffer Optimization. To develop the high-performing SARS-CoV-2 antigen LFA, we optimized the antibody (*i.e.*, antibody pair and amount) and buffer for maximal SB and minimal NSB. For quantitative optimization, NSB was measured by the noise from the test line when testing a blank buffer (*i.e.*, negative controls), while SB was characterized by the signal from the test line when testing an antigen-loaded buffer (*i.e.*, positive controls). First, the antibody pair was optimized for maximal SB. Figure 3A compares the signals of SB between LFAs using two antibody pairs with a controlled amount of GNSs per LFA and with a controlled SARS-CoV-2 spike receptor-binding domain (RBD) antigen concentration in buffer. The first antibody pair gained a much higher SB signal than the second pair, while both assays showed invisible test lines for blank buffer testing. To optimize the running buffer, we, therefore, proceeded with the first pair. NSB was first minimized to preclude any visible false positives, and the specific-to-nonspecific binding ratio (SB/NSB) was then maximized.[42] The testing ranges of pH (7−9), bovine serum albumin (BSA, 0.5−2%), and Triton X-100 (0.5−2%) to optimize the running buffer were selected based on our previous LFA studies using ~100 nm GNSs.[41,42] Figure 3B shows that NSB was quite sensitive to buffer pH and that minimal NSB noise occurred at pH 9. Figure 3C shows that 0.5−1% BSA offered good assay performance, whereas a higher concentration (2%) led to stronger NSB. Figure 3D suggests that 0.5% Triton was optimal with the highest SB/NSB while further increasing Triton reduced SB/NSB. Based on the abovementioned optimization, the optimal template of running buffer for the first antibody pair was 60 mM Tris−HCl buffer (pH 9), 0.5% BSA, 0.5% Triton X-100, 0.15 M NaCl, and 0.05% ProClin 300. Finally, the concentration of the capture antibody precoated at test lines was optimized. Figure 3E suggests that increasing the capture antibody's concentration significantly increased the SB/NSB ratio since the reaction rate of SB increased with the concentration of the reactant. There might be a maximal SB/NSB value at a higher concentration of the capture antibody. However, note that, considering the assay cost and the concentration limit of the as-received antibody (2.4 mg/mL), a 2 mg/mL concentration was used for the precoating capture antibody, although a higher concentration may increase the SB/NSB.

LFA Redesign II: Larger GNSs Improve Visual and Thermal Contrast and Specific Binding. Larger GNSs (120 nm) were used as labels for stronger visual and thermal contrast of a positive test line and higher SB in the assay. The large GNS can improve visual and thermal contrast by its large absorption cross section within the visible range (380−700 nm). The visual reading of a positive test line depends on the scattering contrast of visible light between the test line and background regions of the membrane, while the thermal contrast relies on the absorption contrast at 532 nm (*i.e.*, laser's wavelength in TCA reader). The bare membrane scatters strongly but absorbs weakly within the visible range. When loaded with visible-light absorbers (*e.g.* GNSs), however, strong scattering reduction and absorption enhancement for the membrane were observed, which induced visible and thermal contrast, respectively.[47] By Mie theory calculation,[48] Figure 4A shows that larger GNSs (120 nm) had a much

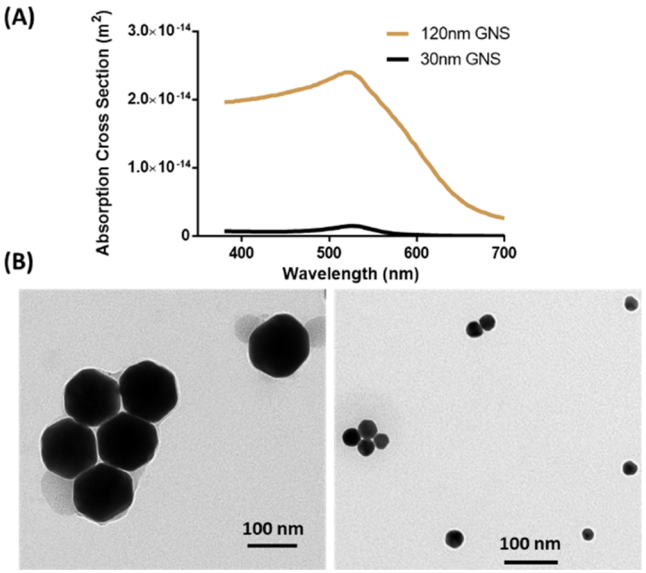

Figure 4. (A) Absorption cross-sectional curves of 120 and 30 nm GNSs in the visible range (380−700 nm). (B) TEM images of 120 and 30 nm GNSs.

stronger absorption of visible light than smaller ones (30 nm), indicating larger visual and thermal contrast for the controlled GNS amount. Their TEM images are shown in Figure 4B. In addition, 120 nm GNSs can achieve more SB at test lines than smaller GNSs due to increased antibody loading capacity, as seen with the 100 nm GNSs used in our previous study.[41] The reaction rate constant for each GNS in SB is proportional to the available binding sites on its surface.[49] Compared with smaller GNSs, larger GNSs with larger surface areas can load more antibodies and therefore have more antigen-binding sites, thus producing more SB in the assay. Based on this consideration, 120 nm GNSs were used throughout the design of the advanced SARS-CoV-2 antigen LFAs below, instead of the smaller ones (20−40 nm) more prevalent in traditional LFAs.

LFA Redesign III: Covalent Conjugation with Increased Antigen-Binding Sites Improves Sensitivity. Physical adsorption (Figure 5A) has been widely used to conjugate GNSs with detection antibodies due to its simplicity and ease of scaling up. For even better LFA performance, we explored the covalent conjugation method (Figure 5A), hypothesizing that this could lead to more active antigen-binding sites from coated antibodies and therefore a higher more SB.

https://doi.org/10.1021/acsanm.1c03217
ACS Appl. Nano Mater. 2021, 4, 13826−13837

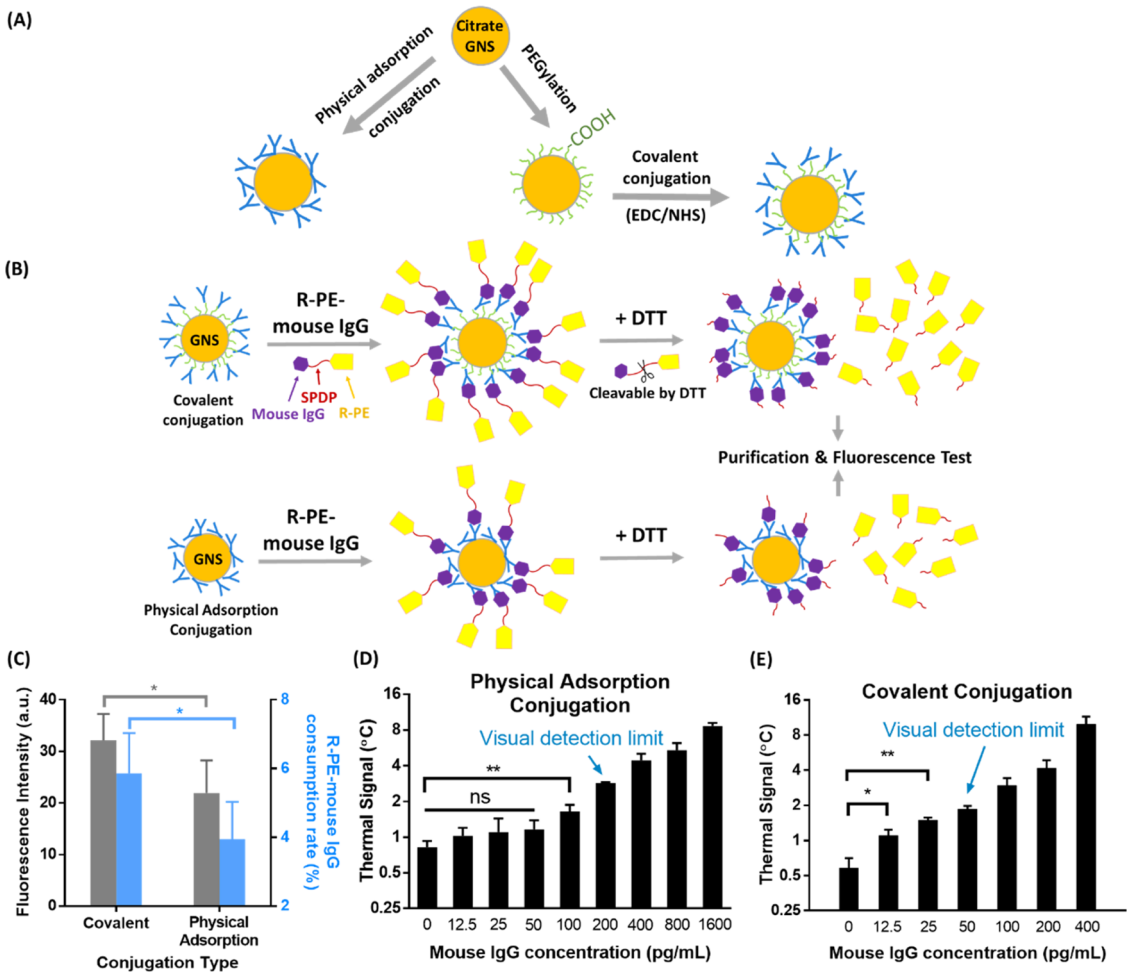

Figure 5. Comparing the covalent *vs* physical adsorption conjugation methods. (A) Schematic of physical adsorption and covalent conjugation methods. (B) Schematic of characterizing active antigen-binding sites from GNS conjugates prepared by covalent and physical adsorption conjugation methods. The GNS−antibody conjugates first reacted with R-phycoerythrin (R-PE)−antigen (*i.e.*, mouse IgG) conjugates to label antigen-binding sites with fluorophores (*i.e.*, R-PE). The R-PE was then released from the GNS−antibody−antigen−RPE complex by dithiothreitol (DTT) cleavage of the disulfide bond between R-PE and antigen, which was provided by a cross-linker, succinimidyl 3-(2-pyridyldithio)propionate (SPDP). The released R-PEs were then measured by a fluorimeter and indicated the binding site amount from GNS conjugates. (C) Normalized fluorescent intensities of released R-PEs post DTT cleavage on the GNS−antibody−antigen−RPE complexes, and normalized R-PE−antigen consumption rates (= bond R-PE-antigen/total addition) in the reaction between GNS conjugates and R-PE−antigen conjugates. The intensities were normalized by GNS amounts from the two conjugation types (~15% difference). (D) Thermal signals of the test lines of mouse IgG LFAs using physical adsorption conjugation. (E) Thermal signals of the test lines of mouse IgG LFAs using covalent conjugation. The data shown in panels C−E were all based on the model antibody and antigen, *i.e.*, goat antimouse IgG antibody (No. M8642, Sigma-Aldrich) and mouse IgG (No. I5381 Sigma-Aldrich). Except for the difference in conjugation methods, other parameters were controlled as the same, including the detection antibody and amount (5 μg per mL of stock GNS solution), LFA strips, running buffer, and TCA reading parameters. The statistical significance is indicated with asterisks: ns: $p > 0.05$; *$p < 0.05$; and **$p < 0.01$.

To test this hypothesis, we conducted binding site characterization by fluorescence measurement (Figure 5B), showing more active antigen-binding sites on covalent GNS conjugates than physical adsorption ones (Figure 5C). To achieve this, a model antigen, mouse IgG, was labeled by a fluorophore (R-phycoerythrin, R-PE) through a cross-linker, which provided a cleavable disulfide bond. After antigen−antibody binding between GNS−antibody conjugates and R-PE−antigen conjugates, the fluorophores were released from the GNS complexes and measured as a representation of antigen-binding sites by the two methods (Figure 5B). The excess free R-PE−antigen conjugates were separated from GNSs and measured. As compared in Figure 5C, the fluorescent intensity (normalized by GNS amount) standing for antigen-binding sites from covalent conjugation was about 46% higher than that from physical adsorption conjugation. A similar difference was seen in the R-PE−antigen consumption rate (= bond R-PE-antigen/total addition) for the antigen−antibody reaction in Figure 5C. This increase in antigen-binding sites might be due to better coating efficiency and/or oriented antibodies in covalent conjugation compared with physical adsorption.

To further verify the hypothesis in an LFA format, model mouse IgG LFAs were developed; these showed better analytical performance by covalent conjugation than physical adsorption. As shown in Figure 5D,E, the physical adsorption had a higher background thermal noise (~0.8 °C) than the covalent one (~0.6 °C). With TCA reading, the LoD for mouse IgG in buffer by covalent conjugation (12.5 pg/mL, 0.08 pM) was about eightfold lower than that by physical

https://doi.org/10.1021/acsanm.1c03217
ACS Appl. Nano Mater. 2021, 4, 13826−13837

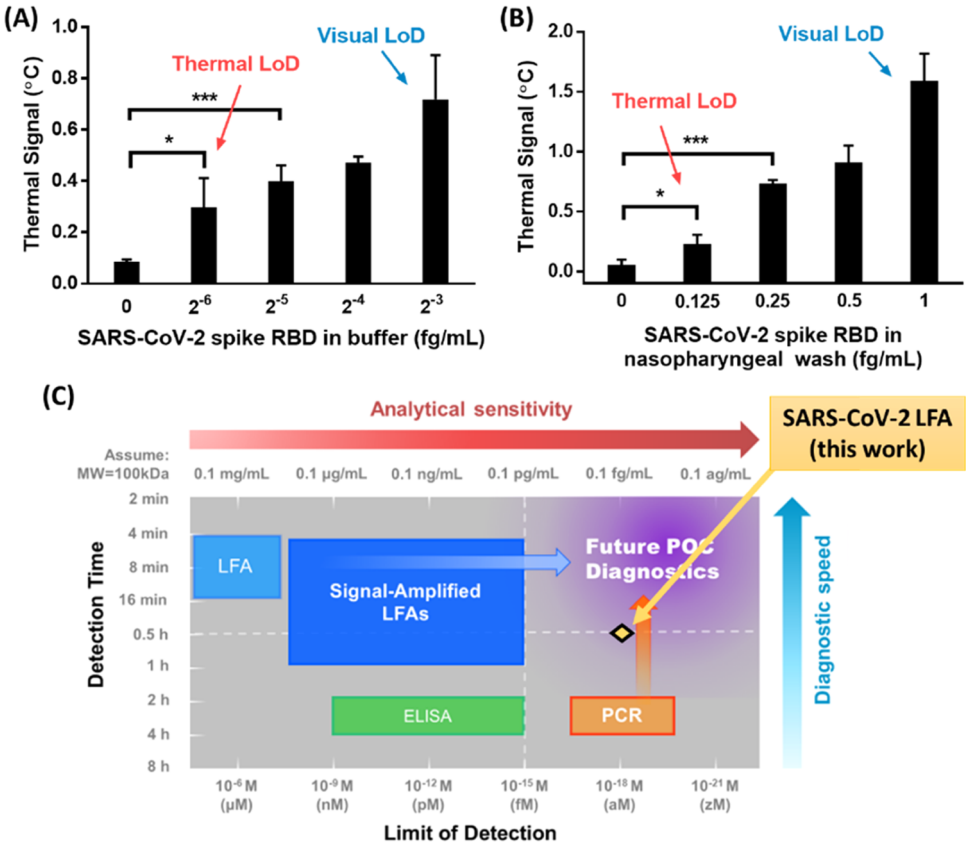

Figure 6. Analytical performance of the SARS-CoV-2 spike receptor-binding domain (RBD) protein LFA with TCA. (A) Thermal signals of test lines to test RBD proteins in running buffer. (B) Thermal signals of test lines to test RBD proteins in the pooled human nasopharyngeal wash. The covalent conjugation was used to prepare those LFAs. (C) Comparing detection sensitivity and assay time of the advanced LFA from this work with other literature work summarized in the previous perspective.[21] Panel C was reproduced from ref 21. Copyright 2021 American Chemical Society. The statistical significance is indicated with asterisks: ns: $p > 0.05$; *$p < 0.05$; **$p < 0.01$; and ***$p < 0.001$.

adsorption (100 pg/mL, 0.7 pM). The LFA samples are shown in Figure S2A.

Above all, compared to physical adsorption conjugation, covalent conjugation had more active antigen-binding sites on the GNS surface and improved analytical sensitivity (*i.e.*, lower LoD) of LFAs. Therefore, in developing SARS-CoV-2 antigen LFAs, covalent conjugation was used, aiming for better sensitivity.

New SARS-CoV-2 TCA LFA: fM−aM Detection Sensitivity of Spike RBD. Based on the abovementioned optimization, we developed the new SARS-CoV-2 spike RBD protein LFA, which demonstrated fM−aM detection sensitivity for the RBD antigen in buffer and human nasopharyngeal wash fluids. When testing serial dilutions of RBD protein in running buffer (in Figure 6A), the visual LoD was 2^{-3} fg/mL (3.6 aM). With TCA reading, subvisual positives were detected, which further lowered the LoD by eightfold down to 2^{-6} fg/mL (0.45 aM). To assess the impact of working in clinical samples, the RBD protein was spiked into the human nasopharyngeal wash, which was collected during the 2017−2018 influenza season without SARS-CoV-2, and then compared with buffer solutions. Here, the LoDs increased by eightfold for both visual and TCA readout, which was 1 fg/mL (28.6 aM) and 2^{-3} fg/mL (3.6 aM), respectively. The LFA samples are shown in Figure S2B. This reduced sensitivity in nasopharyngeal wash compared to clean buffer was probably due to the abundant proteins present in the wash, which might have interacted with and covered certain binding sites from detection and capture antibodies in the assay; the SB could thus have been lowered to a certain extent by the nasopharyngeal wash. Fortunately, there were limited cross-reactions between the antibodies with influenza and other nontargeted proteins from the nasopharyngeal wash because the background noise from testing the unmodified nasopharyngeal wash sample was on a similar level to that from clean buffer, as shown in Figure 6B. This also indicates good specificity of the chosen antibody pair. In addition, the semiquantitative thermal signals from TCA in Figure 6A,B, which were proportional to GNS concentrations at test lines, could be used to indicate the concentrations of RBD analyte in samples.

In terms of SARS-CoV-2 diagnosis, our advanced SARS-CoV-2 spike RBD protein LFA showed much lower LoDs both visually and thermally over literature work, as shown in Table 1. This increased sensitivity by visual reading was mainly due to the high affinity of the antibodies (high SB), optimal running buffer (high SB and low NSB), improved antibody−GNS conjugation methods leading to more antigen-binding sites (high SB), and the use of 120 nm GNSs (strong visual and thermal contrast, high SB). To gain a broader perspective of diagnosis, its performance was compared with other diagnostic platforms summarized in our previous perspective,[21] as shown in Figure 6C. Although its assay time was about 30 min, the advanced LFA in this study showed significant improvement in sensitivity over conventional LFAs and also broke through the detection limits of most previously published signal-amplified LFAs (≥fM). A deeper under-

https://doi.org/10.1021/acsanm.1c03217
ACS Appl. Nano Mater. 2021, 4, 13826−13837

standing of this high detection sensitivity can be achieved through kinetic analysis of the reaction and flow in assay development, which is detailed in Section S5 in the Supporting Information. Briefly, the analysis shows it was the SB of this advanced LFA that was significantly enhanced through those assay optimization steps described above, especially when testing low-concentrated analytes.

CONCLUSIONS

To achieve ultrasensitive diagnostics, an advanced LFA based on GNSs with a TCA diagnostic platform was developed and reported for rapid and highly sensitive testing of the SARS-CoV-2 antigen. In the assay design, comprehensive assay optimization for enhanced SB coupled with signal amplification (TCA) on GNSs was carried out, including high-affinity antibody pair, optimal buffer condition, use of large (120 nm) GNSs, and covalent conjugation. The improved covalent conjugation increased active antigen-binding sites by ∼46% compared with the traditional physical adsorption. The advanced LFA with only visual reading could detect 3.6 and 28.6 aM SARS-CoV-2 spike RBD protein in buffer and human nasopharyngeal wash, respectively. This advanced LFA showed lower visual and thermal LoDs over other literature work in diagnosing SARS-CoV-2. As for the broad view of diagnostics, its detection sensitivity was also much better than conventional LFAs and even comparable to PCR. A fast (<1 min) TCA reading was also developed, which could distinguish 26−32% visual false negatives in clinical commercial LFAs. When applying this TCA to the advanced LFA, another eightfold improvement in sensitivities was achieved, reaching 0.45 aM (in buffer) and 3.6 aM (in the human nasopharyngeal wash) with a semiquantitative readout. Future work is required to further validate both the sensitivity and specificity of the advanced LFA in a cohort or clinical study before commercialization and large-scale production.

MATERIALS AND METHODS

Materials. Chloroauric acid (No. G4022), hydroquinone (No. H9003), poly(ethylene glycol) 2-mercaptoethyl ether acetic acid (SH-PEG2100-COOH, average M_n 2100, No. 757829), bovine serum albumin (BSA, No. A7906), ovalbumin (No. A5503), *N*-hydroxysuccinimide (NHS), potassium phosphate dibasic (No. 795496), potassium phosphate monobasic (No. 795488), Tween 20 (No. P1379), Triton X-100 (laboratory grade), trizma hydrochloride (No. T3252), trizma base (No. T1503), MES monohydrate (No. 69892), goat antimouse IgG antibody (No. M8642), goat antihuman IgG antibody (No. I1011), and mouse IgG (No. I5381) were purchased from Sigma-Aldrich. Sodium citrate (ACS grade) and sucrose (ACS grade) were produced by Macron Fine Chemicals. *N*-(3-Dimethylaminopropyl)-*N*′-ethylcarbodiimide hydrochloride (EDC, No. PG82079), pyridyl disulfide-derivative R-phycoerythrin (R-PE, No. P806, 1.0 average pyridyl disulfide residues per molecule), succinimidyl 3-(2-pyridyldithio)propionate (SPDP, No. 21857), and 10X phosphate-buffered saline (PBS) were purchased from Thermo Fisher Scientific. Dithiothreitol (DTT, No. BP172−5) was purchased from Fisher Scientific. A customized 5X PBS-EDTA buffer (No. BM-682, 1X buffer: 10.1 mM Na2HPO4, 1.8 mM KH2PO4, 137 mM NaCl, 2.7 mM KCl, 10 mM EDTA disodium dihydrate) was produced by Boston Bioproducts. *N*-Hydroxysulfosuccinimide sodium salt (sulfo-NHS, No. 12831) was purchased from Chem Impex. The chimeric antibodies to SARS-CoV-2 spike RBD protein (Nos. RBD5324 and RBD5308) were purchased from Hytest (Finland). The recombinant SARS-CoV-2 spike RBD protein (35 kDa) was purchased from Dr. Fang Li's lab at the University of Minnesota. The polyclonal antimouse IgG antibody and mouse IgG protein were gifted from James Sackrison (from Scantibodies, Inc.). The glass fiber conjugate pad (No. GFCP203000) and nitrocellulose membrane (No. HF 13502XSS) were purchased from EMD Millipore. The wicking pad (No. CF5) was purchased from Cytiva.

TCA: Developing the Fast-Reading Algorithm. To increase the throughput of the TCA reading, we developed a continuous reading algorithm, which allowed it to finish one reading as fast as <1 min. During continuous reading, the laser scanned continuously across a test line (see Figure 1D). The laser and the IR sensor were turned on and kept still while the LFA strip being read was moved at a constant speed controlled by a linear motor. After this reading, a continuous temperature curve was obtained and the area under this curve (AUC) was calculated as its thermal signal. According to the IUPAC method, the detection limit was determined as the lowest analyte concentration in a serial dilution study, whose thermal signal was larger than the summation of mean and 3 times the standard deviation of the thermal signals from blank samples (or negative controls). Meanwhile, the ANOVA analysis of signals from blank and low-analyte samples should show a p-value <0.05.

Clinical Commercial SARS-CoV-2 LFAs for TCA Reading. Clinical samples of nasopharyngeal swabs in viral transport media were collected by healthcare workers during mass testing of unexposed asymptomatic residents in northeast Spain (Metropolità Nord).[50] RT-qPCR tests were performed on these fresh samples stored at 2−8 °C within 24 h, followed by commercial rapid SARS-CoV-2 antigen LFAs from five commercial brands within the next 12 h.[50] The visual readout (±) of rapid tests was compared to PCR results, which were viewed as true results.[50] More details about the clinical sample collection and testing procedures are provided in the recent publication.[50]

To understand how TCA helps improve the sensitivity of commercial SARS-CoV-2 LFAs, some of the commercial LFAs were left to dry after testing and were later transported from Spain to the University of Minnesota (UMN) for TCA reading, as shown in Figure 2A. They included 54 LFAs from the PanBio SARS-CoV-2 Ag Rapid test by Abbott and 53 from the CLINITEST Rapid SARS-CoV-2 Antigen Test by Siemens. These LFAs were selected to consist of mostly visual false negatives, a small portion of true positives and true negatives, and none or a few false positives. To dry these LFAs, the sample, conjugation, and wicking pads were removed to stop any further flow and reaction of reagents for most LFAs, except for a few which had very clear backgrounds after assay completion. The dried LFAs were kept and shipped in a bag with desiccants for further TCA reading with a continuous reading algorithm. An LFA was determined as thermally positive or negative via TCA reading by comparing its thermal signal to a cutoff threshold, which was set as the summation of the mean and 3 times the standard deviation of thermal signals from four PCR-negative samples (true negatives). The correctness (true or false) of thermal and visual results (±) was determined by comparison to PCR results (±) obtained during the clinical study in Spain.

LFA Development I: Screening the SARS-CoV-2 Antibody Pair. The antibody pairs from Hytest and MyBioSource were tested in a lateral flow format and their SB signals were quantified. The capture antibodies and secondary antibodies to detection antibodies were pipetted onto the nitrocellulose membrane as test and control dots at a 1 mg/mL concentration. The membrane was dried in a vacuum overnight prior to assembly and cutting. Corresponding detection antibodies were conjugated with GNSs by the physical adsorption at preoptimized pH with a controlled concentration. The pH of the running buffer was optimized to 9 for both antibody pairs to minimize false positives when testing the blank buffer. To quantify the SB signal, the same positive controls (*i.e.*, the same concentration of SARS-CoV-2 spike RBD protein in buffer) were tested by LFAs using the two antibody pairs. The positive signals were analyzed by plotting grayscale curves across test lines using ImageJ software and the areas above the grayscale curve were calculated for quantitative SB comparison.

LFA Development II: Synthesizing and Characterizing GNSs. The 120 nm GNSs were synthesized by the seed-mediated

https://doi.org/10.1021/acsanm.1c03217
ACS Appl. Nano Mater. 2021, 4, 13826−13837

growth method.[51] Briefly, 15 nm seeds were synthesized according to the method described by Frens et al.[52] First, 1 mL fresh 3.3% (w/v) sodium citrate was added to 100 mL of a boiling 0.25 mM $HAuCl_4$ solution under vigorous stirring. Boiling and stirring were continued for another 10−15 min. The seed solution was cooled to room temperature and diluted to 100 mL with milli-Q ultrapure water for further use or stock. The 120 nm GNSs were then synthesized by adding 1 mL of 0.25 mM $HAuCl_4$, 1 mL of 15 mM sodium citrate, 0.3 mL of seed solution, and 1 mL of 0.25 mM hydroquinone into 97.66 mL of water under vigorous stirring in quick succession. Stirring was kept for at least 2 h at room temperature to complete the growth of GNSs. The GNSs were stabilized by adding Tween 20 at a final concentration of 0.05% (v/v) before storage at 2−8 °C. After synthesis, GNSs were characterized by an ultraviolet−visible−near-infrared (UV−vis−NIR) spectrophotometer (Cary 5000 UV−vis−NIR) and a transmission electron microscope (TEM, Tecnai G2). The concentration of GNSs was determined by Beer's law, where the molar extinction coefficient (ε, $M^{-1}\cdot cm^{-1}$) of GNSs was estimated as[51]

$$\varepsilon = 10^{1.0463\times\log\log(\frac{3}{2}\times\pi\times(\text{diameter}))+4.0935}$$

LFA Development III: Conjugating GNSs with Detection Antibodies. *Physical Adsorption Conjugation.* The stock GNSs were centrifuged once and resuspended in ultrapure water, whose pH was adjusted to near the isoelectric point of detection antibodies by adding 0.2 M K_2CO_3. For model mouse IgG assay, a goat antimouse IgG antibody (M8642, Sigma-Aldrich) was added into GNS solutions at 5 μg per mL GNS at a stock concentration, immediately followed by vortexing and incubation on a rotator at room temperature for 1.5 h. To block the free GNS surface, BSA was added to a final concentration of 1% (w/v), followed by rotating incubation for 0.5 h at room temperature. The GNS−antibody conjugates were centrifuged and washed once by 5 mM PB buffer. Finally, the conjugates were recovered in resuspension buffer (10 mM PB, pH 7.4, 3% (w/v) sucrose, 0.5% (w/v) BSA, 0.05% (v/v) Proclin 300) and stored at 4 °C until further use.

Covalent Conjugation. The stock GNSs were centrifuged once and resuspended in ultrapure water at a fivefold concentration of its stock solution. SH-PEG2100-COOH was added into the GNS solution until a final concentration of 0.75% (w/v). The mixture was stirred vigorously overnight at room temperature to complete the reaction. The PEGylated GNSs were washed three times and resuspended in 10 mM MES buffer for covalent conjugation with antibodies through EDC/NHS chemistry. In 600 μL of a GNS solution, 6 μL of a fresh EDC solution (10 mg/mL) and 12 μL of a fresh sulfo-NHS solution (10 mg/mL) were added and vortexed vigorously, followed by rotation for 30 min at room temperature. The EDC-activated GNSs were washed once to remove excess EDC and sulfo-NHS, resuspended in 5 mM PB buffer (pH 7.2), and incubated with antibodies for 1.5 h at room temperature under rotating. BSA was then added to a final concentration of 1% (w/v) to block the GNS surface, followed by rotation for 0.5 h at room temperature. To ensure sufficient blocking of excess active carboxyl groups on the GNS surface, 12 μL of 12.5% (wt) hydroxylamine was added and incubated for 10 min at room temperature. Finally, the conjugates were washed twice, recovered in resuspension buffer (same as physical adsorption), and stored at 4 °C until further use. Overall, 5 and 10 μg per mL stock GNS of goat antimouse IgG antibody (M8642, Sigma-Aldrich) and antispike RBD antibody (RBD5324, Hytest), respectively, were used in covalent conjugation. The antispike RBD antibody was predialyzed to remove sodium azide before the conjugation steps.

For both conjugation types, the characterization of antigen-binding sites is described in Section S4 in the Supporting Information.

LFA Development IV: Fabricating and Running LFAs. The method to fabricate and perform LFA generally followed our previous studies.[41,42] Briefly, capture antibodies were precoated onto the nitrocellulose membrane by a dispenser (ClaremontBio, Automated Lateral Flow Reagent Dispenser). For the model mouse IgG LFA, an antimouse IgG antibody and mouse IgG (both from Scantibodies, Inc.) were dispensed at 1 and 0.2 mg/mL as test and control lines, respectively. For the SARS-CoV-2 spike LFA, an antispike antibody (No. RBD5308, Hytest) and a goat antihuman IgG antibody (I1011, Sigma-Aldrich) were dispensed at 2 and 0.2−0.4 mg/mL as test and control lines, respectively. Post precoating, the membrane was dried overnight in vacuum at room temperature to immobilize proteins. The conjugate pad, membrane, and absorbent pad were assembled onto an adhesive backing card, with 1−2 mm overlapping between adjacent components to facilitate solution migration. The assembly was laminated and cut into strips 3 mm wide. To run the assay, the LFA strips were dipped into a 96-well plate filled with 140 μL of the sample or buffer solutions. The visual results were recorded after 20 min (mouse IgG LFA) or 30 min (SARS-CoV-2 spike RBD LFA) until completed migration of most GNSs before TCA reading. The number of replication of LFAs for the same condition was three.

SARS-CoV-2 TCA LFA: Testing RBD in the Human Nasopharyngeal Wash. To acquire LFAs' analytical sensitivity for an antigen in human samples, the recombinant SARS-CoV-2 spike RBD protein was spiked into the human nasopharyngeal wash. This wash was collected in the 2017−2018 flu season, pooled from multiple deidentified patients, and stored at −80 °C prior to use.[43] Although some of those patients were diagnosed with influenza A and B infections, the nasopharyngeal wash was void of SARS-CoV-2 infections and thus appropriate for the dilution study of the SARS-CoV-2 spike RBD protein. The recombinant RBD protein was serially diluted by the stock nasopharyngeal wash at different concentrations. Per 1 mL of the RBD-diluted nasopharyngeal wash, 100 μL of running reagents (0.59M Trizma base, 0.39 M Trizma HCl, 5.4% BSA, 8.7% Triton X-100, 1.1% proclin 300) was added and mixed by shaking before each assay test. To run LFAs, the strips were dipped in a 96-well plate filled with 140 μL of the nasopharyngeal wash mixed with running reagents. The assay took about 30 min before visual reading followed by a TCA scan. The number of replication of LFAs for each condition was three.

■ ASSOCIATED CONTENT

Supporting Information

The Supporting Information is available free of charge at https://pubs.acs.org/doi/10.1021/acsanm.1c03217.

More details on the TCA fast-reading algorithm, TCA reading of commercial tests, mouse IgG and advanced SARS-CoV-2 antigen lateral flow immunoassays (LFAs), antigen-binding site characterization, and flow and reaction kinetic analysis of the advanced LFAs (PDF)

■ AUTHOR INFORMATION

Corresponding Author

John C. Bischof − *Department of Mechanical Engineering and Department of Biomedical Engineering, University of Minnesota, Minneapolis, Minnesota 55455, United States;* orcid.org/0000-0001-6726-7111; Email: bischof@umn.edu

Authors

Yilin Liu − *Department of Mechanical Engineering, University of Minnesota, Minneapolis, Minnesota 55455, United States;* orcid.org/0000-0002-8521-8943

Li Zhan − *Department of Mechanical Engineering, University of Minnesota, Minneapolis, Minnesota 55455, United States*

Jesse W. Shen − *Department of Mechanical Engineering, University of Minnesota, Minneapolis, Minnesota 55455, United States*

Bàrbara Baro − *ISGlobal, Hospital Clínic, Universitat de Barcelona, Barcelona 08036, Spain*

Andrea Alemany − *Fight AIDS and Infectious Diseases Foundation, Badalona 08916, Spain; Hospital Universitari Germans Trias i Pujol, Badalona 08916, Spain*

https://doi.org/10.1021/acsanm.1c03217
ACS Appl. Nano Mater. 2021, 4, 13826−13837

James Sackrison − *3984 Hunters Hill Way, Minnetonka, Minnesota 55345, United States*
Oriol Mitjà − *Fight AIDS and Infectious Diseases Foundation, Badalona 08916, Spain; Hospital Universitari Germans Trias i Pujol, Badalona 08916, Spain; Lihir Medical Centre − International SOS, Lihir Island, New Ireland 633, Papua New Guinea*

Complete contact information is available at: https://pubs.acs.org/10.1021/acsanm.1c03217

Notes

The authors declare the following competing financial interest(s): John Bischof is a founder and James Sackrison is a consultant of Vigilant Diagnostics. This company is focused on the commercialization of thermal contrast amplification readers and lateral flow assays.

■ ACKNOWLEDGMENTS

This work was supported by the National Science Foundation (CBET- 2029474). J.C.B. acknowledges the Kuhrmeyer Chair in Mechanical Engineering and the Medtronic-Bakken Endowed Chair for Engineering in Medicine. The authors gratefully acknowledge a seed grant from the University of Minnesota (UMN) Medical school to develop SARS-CoV-2 diagnostics. B.B. is a Beatriu de Pinós postdoctoral fellow granted by the Government of Catalonia's Secretariat for Universities and Research and by the Marie Sklodowska-Curie Actions COFUND Programme (BP3, 801370). This work was also supported by internal funds from Fundació Institut d'Investigació en Ciències de la Salut Germans Trias i Pujol and #YoMeCorono.org crowdfunding campaign. The fluorescence tests were performed at the Biophysical Technology Center, Department of Biochemistry, Molecular Biology, and Biophysics at UMN. TEM imaging was carried out in the Characterization Facility, UMN. The authors thank Dr. Guebum Han and Dr. Michael McAlpine for helping print gold nanoparticle solutions onto the membrane in preparing calibration strips, Dr. Zhe Gao for acquiring TEM images and helpful discussion on chemical reactions, Dr. Wei Shen for giving Y.L. and J.W.S access to the spectrophotometer, Dr. David Boulware for the helpful discussion on clinical samples and tests, Jacqueline Pasek-Allen for the helpful discussion on the PEGylation reaction, and Laura Bischof and Susan Everson for their help with writing improvement.

■ REFERENCES

(1) Wang, C.; Horby, P. W.; Hayden, F. G.; Gao, G. F. A Novel Coronavirus Outbreak of Global Health Concern. *Lancet* **2020**, *395*, 470−473.
(2) Zhu, N.; Zhang, D.; Wang, W.; Li, X.; Yang, B.; Song, J.; Zhao, X.; Huang, B.; Shi, W.; Lu, R.; Niu, P.; Zhan, F.; Ma, X.; Wang, D.; Xu, W.; Wu, G.; Gao, G. F.; Tan, W. A Novel Coronavirus from Patients with Pneumonia in China, 2019. *N. Engl. J. Med.* **2020**, *382*, 727−733.
(3) Broughton, J. P.; Deng, X.; Yu, G.; Fasching, C. L.; Servellita, V.; Singh, J.; Miao, X.; Streithorst, J. A.; Granados, A.; Sotomayor-Gonzalez, A.; Zorn, K.; Gopez, A.; Hsu, E.; Gu, W.; Miller, S.; Pan, C. Y.; Guevara, H.; Wadford, D. A.; Chen, J. S.; Chiu, C. Y. CRISPR−Cas12-Based Detection of SARS-CoV-2. *Nat. Biotechnol.* **2020**, *38*, 870−874.
(4) WHO. *COVID-19 Weekly Epidemiological Update 35*; World Health Organization, No. December, 2021; pp 1−3.
(5) Udugama, B.; Kadhiresan, P.; Kozlowski, H. N.; Malekjahani, A.; Osborne, M.; Li, V. Y. C.; Chen, H.; Mubareka, S.; Gubbay, J. B.; Chan, W. C. W. Diagnosing COVID-19: The Disease and Tools for Detection. *ACS Nano.* **2020**, *14*, 3822−3835.
(6) Yadav, S.; Sadique, M. A.; Ranjan, P.; Kumar, N.; Singhal, A.; Srivastava, A. K.; Khan, R. SERS Based Lateral Flow Immunoassay for Point-of-Care Detection of SARS-CoV-2 in Clinical Samples. *ACS Appl. Bio Mater.* **2021**, *4*, 2974−2995.
(7) Osborn, M. J.; Bhardwaj, A.; Bingea, S. P.; Knipping, F.; Feser, C. J.; Lees, C. J.; Collins, D. P.; Steer, C. J.; Blazar, B. R.; Tolar, J. CRISPR/Cas9-Based Lateral Flow and Fluorescence Diagnostics. *Bioengineering* **2021**, *8*, 23.
(8) Borst, A.; Box, A. T. A.; Fluit, A. C. False-Positive Results and Contamination in Nucleic Acid Amplification Assays: Suggestions for a Prevent and Destroy Strategy. *Eur. J. Clin. Microbiol. Infect. Dis.* **2004**, *23*, 289−299.
(9) Oladipo, E. K.; Ajayi, A. F.; Odeyemi, A. N.; Akindiya, O. E.; Adebayo, E. T.; Oguntomi, A. S.; Oyewole, M. P.; Jimah, E. M.; Oladipo, A. A.; Ariyo, O. E.; Oladipo, B. B.; Oloke, J. K. Laboratory Diagnosis of COVID-19 in Africa: Availability, Challenges and Implications. *Drug Discoveries Ther.* **2020**, *14*, 153−160.
(10) Kusotera, T.; Nhengu, T. G. Coronavirus-19 and Malaria: The Great Mimics. *Afr. J. Primary Health Care Fam. Med.* **2020**, *12*, 1−3.
(11) Serrano, M. M.; Rodríguez, D. N.; Palop, N. T.; Arenas, R. O.; Córdoba, M. M.; Mochón, M. D. O.; Cardona, C. G. Comparison of Commercial Lateral Flow Immunoassays and ELISA for SARS-CoV-2 Antibody Detection. *J. Clin. Virol.* **2020**, *129*, No. 104529.
(12) Li, Z.; Yi, Y.; Luo, X.; Xiong, N.; Liu, Y.; Li, S.; Sun, R.; Wang, Y.; Hu, B.; Chen, W.; Zhang, Y.; Wang, J.; Huang, B.; Lin, Y.; Yang, J.; Cai, W.; Wang, X.; Cheng, J.; Chen, Z.; Sun, K.; Pan, W.; Zhan, Z.; Chen, L.; Ye, F. Development and Clinical Application of a Rapid IgM-IgG Combined Antibody Test for SARS-CoV-2 Infection Diagnosis. *J. Med. Virol.* **2020**, *92*, 1518−1524.
(13) Diao, B.; Wen, K.; Chen, J.; Liu, Y.; Yuan, Z.; Han, C.; Chen, J.; Pan, Y.; Chen, L.; Dan, Y.; Wang, J.; Chen, Y.; Deng, G.; Zhou, H.; Wu, Y. Diagnosis of Acute Respiratory Syndrome Coronavirus 2 Infection by Detection of Nucleocapsid Protein. *medRxiv* **2020**, No. 2020.03.07.20032524.
(14) Albert, E.; Torres, I.; Bueno, F.; Huntley, D.; Molla, E.; Fernández-Fuentes, M. Á.; Martínez, M.; Poujois, S.; Forqué, L.; Valdivia, A.; Solano de la Asunción, C.; Ferrer, J.; Colomina, J.; Navarro, D. Field Evaluation of a Rapid Antigen Test (Panbio COVID-19 Ag Rapid Test Device) for COVID-19 Diagnosis in Primary Healthcare Centres. *Clin. Microbiol. Infect.* **2021**, *27*, 472.e7−472.e10.
(15) Scohy, A.; Anantharajah, A.; Bodéus, M.; Kabamba-Mukadi, B.; Verroken, A.; Rodriguez-Villalobos, H. Low Performance of Rapid Antigen Detection Test as Frontline Testing for COVID-19 Diagnosis. *J. Clin. Virol.* **2020**, *129*, No. 104455.
(16) Perchetti, G. A.; Huang, M. L.; Mills, M. G.; Jerome, K. R.; Greninger, A. L. Analytical Sensitivity of the Abbott BinaxNOW COVID-19 Ag Card. *J. Clin. Microbiol.* **2021**, *59*, e02880−20.
(17) Nagura-Ikeda, M.; Imai, K.; Tabata, S.; Miyoshi, K.; Murahara, N.; Mizuno, T.; Horiuchi, M.; Kato, K.; Imoto, Y.; Iwata, M.; Mimura, S.; Ito, T.; Tamura, K.; Kato, Y. Clinical Evaluation of Self-Collected Saliva by Quantitative Reverse Transcription-PCR (RT-QPCR), Direct RT-QPCR, Reverse Transcription−Loop-Mediated Isothermal Amplification, and a Rapid Antigen Test To Diagnose COVID-19. *J. Clin. Microbiol.* **2020**, *58*, e01438−20.
(18) Prince-Guerra, J. L.; Almendares, O.; Nolen, L. D.; Gunn, J. K. L.; Dale, A. P.; Buono, S. A.; Deutsch-Feldman, M.; Suppiah, S.; Hao, L.; Zeng, Y.; Stevens, V. A.; Knipe, K.; Pompey, J.; Atherstone, C.; Bui, D. P.; Powell, T.; Tamin, A.; Harcourt, J. L.; Shewmaker, P. L.; Medrzycki, M.; Wong, P.; Jain, S.; Tejada-Strop, A.; Rogers, S.; Emery, B.; Wang, H.; Petway, M.; Bohannon, C.; Folster, J. M.; MacNeil, A.; Salerno, R.; Kuhnert-Tallman, W.; Tate, J. E.; Thornburg, N. J.; Kirking, H. L.; Sheiban, K.; Kudrna, J.; Cullen, T.; Komatsu, K. K.; Villanueva, J. M.; Rose, D. A.; Neatherlin, J. C.; Anderson, M.; Rota, P. A.; Honein, M. A.; Bower, W. A. Evaluation of Abbott BinaxNOW Rapid Antigen Test for SARS-CoV-2 Infection at

Two Community-Based Testing Sites — Pima County, Arizona, November 3−17, 2020. *Morb. Mortal. Wkly. Rep.* **2021**, *70*, 100−105.
(19) Crook, D. W.; Screaton, G. R.; Adams, E. R.; Ainsworth, M.; Anand, R.; Andersson, M. I.; Auckland, K.; Baillie, J. K.; Barnes, E.; Beer, S.; Bell, J. I.; Berry, T.; Bibi, S.; Carroll, M.; Chinnakannan, S. K.; Clutterbuck, E.; Cornall, R. J.; de Silva, T.; Dejnirattisai, W.; Dingle, K. E.; Dold, C.; Espinosa, A.; Eyre, D. W.; Farmer, H.; Fernandez Mendoza, M.; Georgiou, D.; Hoosdally, S. J.; Hunter, A.; Jefferey, K.; Kelly, D. F.; Klenerman, P.; Knight, J.; Knowles, C.; Kwok, A. J.; Leuschner, U.; Levin, R.; Liu, C.; López-Camacho, C.; Martinez, J.; Matthews, P. C.; McGivern, H.; Mentzer, A. J.; Milton, J.; Mongkolsapaya, J.; Moore, S. C.; Oliveira, M. S.; Pereira, F.; Perez, E.; Peto, T.; Ploeg, R. J.; Pollard, A.; Prince, T.; Roberts, D. J.; Rudkin, J. K.; Sanchez, V.; Semple, M. G.; Slon-Campos, J.; Skelly, D. T.; Smith, E. N.; Sobrinodiaz, A.; Staves, J.; Stuart, D. I.; Supasa, P.; Surik, T.; Thraves, H.; Tsang, P.; Turtle, L.; Walker, A. S.; Wang, B.; Washington, C.; Watkins, N.; Whitehouse, J. Antibody Testing for COVID-19: A Report from the National COVID Scientific Advisory Panel. *Wellcome Open Res.* **2020**, *5*, 1.
(20) Döhla, M.; Boesecke, C.; Schulte, B.; Diegmann, C.; Sib, E.; Richter, E.; Eschbach-Bludau, M.; Aldabbagh, S.; Marx, B.; Eis-Hübinger, A. M.; Schmithausen, R. M.; Streeck, H. Rapid Point-of-Care Testing for SARS-CoV-2 in a Community Screening Setting Shows Low Sensitivity. *Public Health* **2020**, *182*, 170−172.
(21) Liu, Y.; Zhan, L.; Qin, Z.; Sackrison, J.; Bischof, J. C. Ultrasensitive and Highly Specific Lateral Flow Assays for Point-of-Care Diagnosis. *ACS Nano.* **2021**, *15*, 3593−3611.
(22) Ye, H.; Liu, Y.; Zhan, L.; Liu, Y.; Qin, Z. Signal Amplification and Quantification on Lateral Flow Assays by Laser Excitation of Plasmonic Nanomaterials. *Theranostics* **2020**, *10*, 4359−4373.
(23) Soh, J. H.; Chan, H. M.; Ying, J. Y. Strategies for Developing Sensitive and Specific Nanoparticle-Based Lateral Flow Assays as Point-of-Care Diagnostic Device. In *Nano Today*; Elsevier B.V., Feb 1, 2020; Vol. *30*, p 100831.
(24) Kawasaki, H.; Suzuki, H.; Maekawa, M.; Hariyama, T. Combination of the NanoSuit Method and Gold/Platinum Particle-Based Lateral Flow Assay for Quantitative and Highly Sensitive Diagnosis Using a Desktop Scanning Electron Microscope. *J. Pharm. Biomed. Anal.* **2021**, *196*, No. 113924.
(25) Zhang, C.; Zheng, T.; Wang, H.; Chen, W.; Huang, X.; Liang, J.; Qiu, L.; Han, D.; Tan, W. Rapid One-Pot Detection of SARS-CoV-2 Based on a Lateral Flow Assay in Clinical Samples. *Anal. Chem.* **2021**, *93*, 3325−3330.
(26) Xiong, E.; Jiang, L.; Tian, T.; Hu, M.; Yue, H.; Huang, M.; Lin, W.; Jiang, Y.; Zhu, D.; Zhou, X. Simultaneous Dual-Gene Diagnosis of SARS-CoV-2 Based on CRISPR/Cas9-Mediated Lateral Flow Assay. *Angew. Chem.* **2021**, *133*, 5367−5375.
(27) Zheng, Y. Z.; Chen, J. T.; Li, J.; Wu, X. J.; Wen, J. Z.; Liu, X. Z.; Lin, L. Y.; Liang, X. Y.; Huang, H. Y.; Zha, G. C.; Yang, P. K.; Li, L. J.; Zhong, T. Y.; Liu, L.; Cheng, W. J.; Song, X. N.; Lin, M. Reverse Transcription Recombinase-Aided Amplification Assay With Lateral Flow Dipstick Assay for Rapid Detection of 2019 Novel Coronavirus. *Front. Cell. Infect. Microbiol.* **2021**, *11*, 24.
(28) Shelite, T.; Uscanga-Palomeque, A.; Castellanos, A.; Melby, P.; Travi, B. Isothermal Recombinase Polymerase Amplification-Lateral Flow Detection of SARS-CoV-2, the Etiological Agent of COVID-19. *J. Virol. Methods* **2021**, *296*, No. 114227.
(29) Liu, D.; Shen, H.; Zhang, Y.; Shen, D.; Zhu, M.; Song, Y.; Zhu, Z.; Yang, C. A Microfluidic-Integrated Lateral Flow Recombinase Polymerase Amplification (MI-IF-RPA) Assay for Rapid COVID-19 Detection. *Lab Chip* **2021**, *21*, 2019−2026.
(30) Chen, Z.; Zhang, Z.; Zhai, X.; Li, Y.; Lin, L.; Zhao, H.; Bian, L.; Li, P.; Yu, L.; Wu, Y.; Lin, G. Rapid and Sensitive Detection of Anti-SARS-CoV-2 IgG, Using Lanthanide-Doped Nanoparticles-Based Lateral Flow Immunoassay. *Anal. Chem.* **2020**, *92*, 7226−7231.
(31) Wang, C.; Shi, D.; Wan, N.; Yang, X.; Liu, H.; Gao, H.; Zhang, M.; Bai, Z.; Li, D.; Dai, E.; Rong, Z.; Wang, S. Development of Spike Protein-Based Fluorescence Lateral Flow Assay for the Simultaneous Detection of SARS-CoV-2 Specific IgM and IgG. *Analyst* **2021**, *146*, 3908−3917.
(32) Chen, R.; Ren, C.; Liu, M.; Ge, X.; Qu, M.; Zhou, X.; Liang, M.; Liu, Y.; Li, F. Early Detection of SARS-CoV-2 Seroconversion in Humans with Aggregation-Induced Near-Infrared Emission Nanoparticle-Labeled Lateral Flow Immunoassay. *ACS Nano* **2021**, *15*, 8996−9004.
(33) Liu, H.; Dai, E.; Xiao, R.; Zhou, Z.; Zhang, M.; Bai, Z.; Shao, Y.; Qi, K.; Tu, J.; Wang, C.; Wang, S. Development of a SERS-Based Lateral Flow Immunoassay for Rapid and Ultra-Sensitive Detection of Anti-SARS-CoV-2 IgM/IgG in Clinical Samples. *Sens. Actuators, B* **2021**, *329*, No. 129196.
(34) Peng, T.; Liu, X.; Adams, L. G.; Agarwal, G.; Akey, B.; Cirillo, J.; Deckert, V.; Delfan, S.; Fry, E.; Han, Z.; Hemmer, P.; Kattawar, G.; Kim, M.; Lee, M. C.; Lu, C.; Mogford, J.; Nessler, R.; Neuman, B.; Nie, X.; Pan, J.; Pryor, J.; Rajil, N.; Shih, Y.; Sokolov, A.; Svidzinsky, A.; Wang, D.; Yi, Z.; Zheltikov, A.; Scully, M. Enhancing Sensitivity of Lateral Flow Assay with Application to SARS-CoV-2. *Appl. Phys. Lett.* **2020**, *117*, No. 120601.
(35) Lee, J. H.; Choi, M.; Jung, Y.; Lee, S. K.; Lee, C. S.; Kim, J.; Kim, J.; Kim, N. H.; Kim, B. T.; Kim, H. G. A Novel Rapid Detection for SARS-CoV-2 Spike 1 Antigens Using Human Angiotensin Converting Enzyme 2 (ACE2). *Biosens. Bioelectron.* **2021**, *171*, No. 112715.
(36) Liu, D.; Wu, F.; Cen, Y.; Ye, L.; Shi, X.; Huang, Y.; Fang, S.; Ma, L. Comparative Research on Nucleocapsid and Spike Glycoprotein as the Rapid Immunodetection Targets of COVID-19 and Establishment of Immunoassay Strips. *Mol. Immunol.* **2021**, *131*, 6−12.
(37) Grant, B. D.; Anderson, C. E.; Williford, J. R.; Alonzo, L. F.; Glukhova, V. A.; Boyle, D. S.; Weigl, B. H.; Nichols, K. P. SARS-CoV-2 Coronavirus Nucleocapsid Antigen-Detecting Half-Strip Lateral Flow Assay toward the Development of Point of Care Tests Using Commercially Available Reagents. *Anal. Chem.* **2020**, *92*, 11305−11309.
(38) Qin, Z.; Chan, W. C. W.; Boulware, D. R.; Akkin, T.; Butler, E. K.; Bischof, J. C. Significantly Improved Analytical Sensitivity of Lateral Flow Immunoassays by Using Thermal Contrast. *Angew. Chem., Int. Ed.* **2012**, *51*, 4358−4361.
(39) Boulware, D. R.; Rolfes, M. A.; Rajasingham, R.; von Hohenberg, M.; Qin, Z.; Taseera, K.; Schutz, C.; Kwizera, R.; Butler, E. K.; Meintjes, G.; Muzoora, C.; Bischof, J. C.; Meya, D. B. Multisite Validation of Cryptococcal Antigen Lateral Flow Assay and Quantification by Laser Thermal Contrast. *Emerging Infect. Dis.* **2014**, *20*, 45−53.
(40) Wang, Y.; Qin, Z.; Boulware, D. R.; Pritt, B. S.; Sloan, L. M.; Gonzalez, I. J.; Bell, D.; Rees-Channer, R. R.; Chiodini, P.; Chan, W. C. W.; Bischof, J. C. Thermal Contrast Amplification Reader Yielding 8-Fold Analytical Improvement for Disease Detection with Lateral Flow Assays. *Anal. Chem.* **2016**, *88*, 11774−11782.
(41) Zhan, L.; Guo, S. Z.; Song, F.; Gong, Y.; Xu, F.; Boulware, D. R.; McAlpine, M. C.; Chan, W. C. W.; Bischof, J. C. The Role of Nanoparticle Design in Determining Analytical Performance of Lateral Flow Immunoassays. *Nano Lett.* **2017**, *17*, 7207−7212.
(42) Zhan, L.; Granade, T.; Liu, Y.; Wei, X.; Youngpairoj, A.; Sullivan, V.; Johnson, J.; Bischof, J. Development and Optimization of Thermal Contrast Amplification Lateral Flow Immunoassays for Ultrasensitive HIV P24 Protein Detection. *Microsyst. Nanoeng.* **2020**, *6*, No. 54.
(43) Liu, Y.; Zhan, L.; Wang, Y.; Kangas, J.; Larkin, D.; Boulware, D. R.; Bischof, J. C. Improved Influenza Diagnostics through Thermal Contrast Amplification. *Diagnostics* **2021**, *11*, 462.
(44) Wang, Y.; Louwagie, E.; Larkin, D.; Sankey, S.; Boulware, D. R.; Bischof, J. C. Improved Detection of Group A: Streptococcus during Thermal Contrast Amplification vs. Visual Reading of Clinical Rapid Diagnostic Tests. *Anal. Methods* **2019**, *11*, 2013−2017.
(45) De Puig, H.; Bosch, I.; Carré-Camps, M.; Hamad-Schifferli, K. Effect of the Protein Corona on Antibody-Antigen Binding in

https://doi.org/10.1021/acsanm.1c03217
ACS Appl. Nano Mater. 2021, 4, 13826−13837

Nanoparticle Sandwich Immunoassays. *Bioconjugate Chem.* **2017**, *28*, 230−238.
(46) Lin, L.-K.; Uzunoglu, A.; Stanciu, L. A. Aminolated and Thiolated PEG-Covered Gold Nanoparticles with High Stability and Antiaggregation for Lateral Flow Detection of Bisphenol A. *Small* **2018**, *14*, No. 1702828.
(47) Wang, Y. *Measurement and Application of Heat Generation from Gold Nanoparticle Systems under Laser Irradiation in Biomedicine*; University of Minnesota, 2019.
(48) Oldenburg, S. J. *Light Scattering from Gold Nanoshells*; Rice University, 2000.
(49) Mosley, G. L.; Nguyen, P.; Wu, B. M.; Kamei, D. T. Development of Quantitative Radioactive Methodologies on Paper to Determine Important Lateral-Flow Immunoassay Parameters. *Lab Chip* **2016**, *16*, 2871−2881.
(50) Baro, B.; Rodo, P.; Ouchi, D.; Bordoy, A. E.; Saya Amaro, E. N.; Salsench, S. V.; Molinos, S.; Alemany, A.; Ubals, M.; Corbacho-Monné, M.; Millat-Martinez, P.; Marks, M.; Clotet, B.; Prat, N.; Estrada, O.; Vilar, M.; Ara, J.; Vall-Mayans, M.; G-Beiras, C.; Bassat, Q.; Blanco, I.; Mitjà, O. Performance Characteristics of Five Antigen-Detecting Rapid Diagnostic Test (Ag-RDT) for SARS-CoV-2 Asymptomatic Infection: A Head-to-Head Benchmark Comparison. *J. Infect.* **2021**, *82*, 269−275.
(51) Perrault, S. D.; Chan, W. C. W. Synthesis and Surface Modification of Highly Monodispersed, Spherical Gold Nanoparticles of 50−200 Nm. *J. Am. Chem. Soc.* **2009**, *131*, 17042−17043.
(52) FRENS, G. Controlled Nucleation for the Regulation of the Particle Size in Monodisperse Gold Suspensions. *Nat. Phys. Sci.* **1973**, *241*, 20−22.

https://doi.org/10.1021/acsanm.1c03217
ACS Appl. Nano Mater. 2021, 4, 13826−13837